Biol. Cybern. 78, 227–243 (1998)

Biological Cybernetics

An equivalent cable model for neuronal trees with active membrane

M. Ohme, A. Schierwagen

Institute for Computer Science, University of Leipzig, D-04109 Leipzig, Germany

Received: 25 September 1997 / Accepted: 13 November 1997

Abstract. A non-uniform equivalent cable model of membrane voltage changes in branching neuronal trees with active ion channels has been developed. A general branching condition is formulated, extending Rall's 3/2 power rule for passive dendritic trees so that non-uniform cable segments can be treated. The theoretical results support the use of the dendritic profile model of Clements and Redman. The theory is then applied to dendrites of different morphological type yielding qualitative different response behaviour.

Key words. Non-uniform equivalent cable – Dendritic profile – Reduced neuron model – Dendritic information processing – Active membrane

1 Introduction

The dendrites of cortical neurons contain a variety of voltage-gated channels that may be important to neuronal signal processing. Compartmental models are known to cope not only with any complexity of dendritic branching but also with non-linear membrane properties. The models then contain hundreds of compartments, and thousands of coupled differential equations must be solved at each time step.

To find analytical tools to describe the spatio-temporal response behaviour, or at least to speed up simulations, approximations to branching dendritic trees have been used, i.e. models that preserve important properties of the signal flow but are described by a much smaller number of differential or algebraic equations for easier mathematical or numerical analysis.

In particular, massive synaptic input typical for most neurons can be studied by means of a coarse classification of different input types with respect to input site, kinetic properties, type of synaptic channels, etc. A specific feature of input organization is layering, e.g. in the cortex. The equivalent cable model has characteristics supporting the analysis of the effects of such layered synaptic inputs (Fig. 1). Problems within this frame include: effect of different active dendritic ion channels, influence of relative locations and strength (number, electrical parameter) of synaptic inputs, and impact of different cell morphologies. In this article we will look mainly at the last of these problems for demonstrating the power of the equivalent cable concept.

For passive dendritic trees fulfilling certain symmetry conditions the reduction to an *equivalent cable* can be justified on theoretical grounds (Schierwagen 1994). In several studies the equivalent cable model has been employed for active trees too, albeit in rather heuristic ways (Stratford et al. 1989; Bush and Sejnowski 1993; Mainen and Sejnowski 1996). To provide theoretical justification for such reduced models, we have developed an equivalent cable model for active dendrites. The model generalizes precursor models in two respects: first, the morphological classes of neuronal trees accessible to analytical treatment have been broadened, and second, trees endowed with active membrane have also been customized.[1]

1.1 Procedure

Starting with the general cable model for neuronal processes we present the special cases of neuronal trees with passive and active membrane, respectively. Then we explain the graph-theoretical concept of a tree as used here to represent a neuronal tree. By the phrase 'neuronal tree' we mean both dendrites and axonal arbours. If we use the term 'tree' without further specification, we refer to the graph-theoretical concept of a (labelled, directed) tree that is used here as a mathematical model for all kinds of neuronal trees. This enables us to compare and relate localizations on different tree that segments with respect to functional parameters.

Correspondence to: A. Schierwagen
(e-mail: schierwa@informatik.uni-leipzig.de)

[1] Parts of these results have been published elsewhere (Ohme and Schierwagen 1996b, 1997).

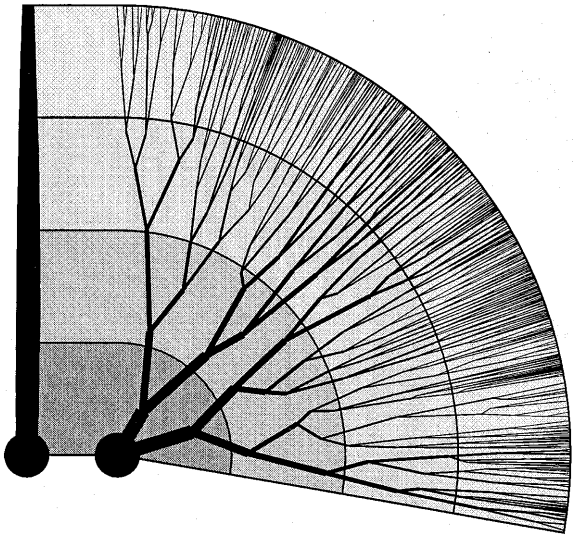

Fig. 1. The reduction of a neuron with two stem dendrites to an equivalent cable. The lines connect points of equal normalized distance on the dendrites and on the non-uniform equivalent cable with a diameter profile corresponding to the cosine function

After these preliminaries, Theorem 1 (Equivalent Cable Theorem) presents the main result of the paper, stating that a neuronal tree fulfilling some linked geometrical and electrical conditions can be reduced to an equivalent cable. We will point out the method used for achieving a dendritic profile approximating to the equivalent cable. For dendritic trees with cylindrical segments this method is equivalent to the dendritic profile model (Fleshman et al. 1988; Clements and Redman 1989; Mainen et al. 1996). The application of this method and of the cartoon representation of dendrites based on it (Stratford et al. 1989), respectively, is further confirmed as both methods give the correct results for trees fulfilling our equivalent cable conditions. In contrast, for the reduced compartmental model used in Bush and Sejnowski (1993) this is not the case. However, their purely heuristic approach could be adapted to yield correct results in the case of an existing equivalent cable while preserving some of their reduction aims.

For illustration purposes, we analyse the signal flow in two neuronal trees (with assumed active membrane) and their dendritic profiles. One fulfils our reduction criteria whereas the other violates some of them, leading, nevertheless, to appropriate results.

In the general case of an equivalent cable, the voltage changes in it have to be further on numerically calculated, representing the cable by just a few compartments. However, some non-uniform equivalent cable profiles admit exact solutions of the dynamic voltage distribution (Schierwagen 1989; Ohme 1996). We employ this result to show analytically the qualitatively different response behaviour caused by synaptic inputs to dendrites of different geometric type.

Finally, we discuss the reduction model, touching on its advantages and drawbacks.

2 General cable model for neuronal segments

The usual mathematical description of the voltage distribution in neuronal trees proceeds from the application of one-dimensional cable theory to the tree segments (Jack et al. 1983). Representing the cable by an RC ladder network (Fig. 2), the cable equation for the transmembrane potential $V(x,t)$ and the axial current $j_a(x,t)$ in a single segment is as follows (x represents distance in axial direction):

$$j_a = -\frac{1}{r_a(x)}\frac{\partial V}{\partial x}, \qquad -\frac{\partial j_a}{\partial x} = j_m = j_c + j_i \tag{1}$$

where $j_m(x,t)$ denotes the membrane current consisting of a capacitive component j_c and a resistive one j_i.

We assume that the current j_i created by the ionic channels in the membrane can be written as a product of a 'resting' conductance $g(x)$ that depends on the membrane surface at x and a non-linear voltage function $f_0(x, V, u_1, \ldots, u_N)$ reflecting the threshold behaviour of the voltage-dependent channels as a specific membrane property (i.e. per unit membrane surface). The latter may be time-dependent so additional variables $u_k(x,t)$ defined by further first-order differential equations have to be included:

$$j_c = c(x)\frac{\partial V}{\partial t} \tag{2a}$$

$$j_i = g(x) f_0(x, V, u_1, \ldots, u_N) \tag{2b}$$

$$\frac{\partial u_k}{\partial t} = f_k(x, V, u_1, \ldots, u_N) \quad \text{for } 1 \le k \le N \tag{2c}$$

Combining (1), (2a) and (2b) we obtain for any segment

$$\frac{\partial}{\partial x}\left(\frac{1}{r_a(x)}\frac{\partial V}{\partial x}\right) = c(x)\frac{\partial V}{\partial t} + g(x) f_0(x, V, u_1, \ldots, u_N) \tag{3}$$

The voltage and current distribution over the whole neuronal tree is described then by a system of second-order partial differential equations (3) that are coupled by their boundary conditions at both ends of the segments.

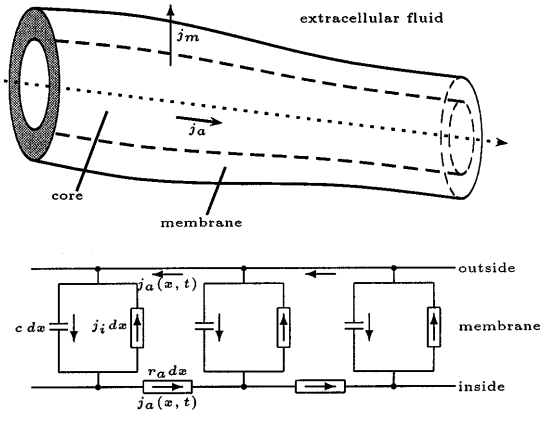

Fig. 2. Flow of current in a nerve fibre segment (core conductor model) and its equivalent electrical circuit

2.1 Specific cable segment models

In most cases the axial resistance $r_a(x)$ is assumed to be inversely proportional to the cross-section of the segment, whereas the membrane conductance $g(x)$ and the membrane capacitance $c(x)$ (all quantities per unit length) are proportional to the membrane surface:

$$r_a(x) = R_i \frac{4}{\pi d(x)^2}$$

$$c(x) = C_m \pi d(x) \sqrt{1 + \frac{1}{4}\left(\frac{dd}{dx}\right)^2} \tag{4}$$

and

$$g(x) = G_m \pi d(x) \sqrt{1 + \frac{1}{4}\left(\frac{dd}{dx}\right)^2}$$

where $d(x)$ denotes the variable cable diameter, R_i the specific intracellular resistance, and C_m and G_m the specific membrane capacitance and 'resting' conductance. The last is the conductance in the nearly linear subthreshold range around the resting potential.

For all the following examples and plausibility consideration we will use the above equations for segments with a circular cross-section. To further simplify the analysis, we assume then $\sqrt{1 + \frac{1}{4}\left(\frac{dd}{dx}\right)^2} \approx 1$, which should be satisfied in most cases. However, the theoretical results derived below apply also to differently chosen r-, g-, and c-functions.

2.1.1 Linear cable. The simplest cable model (no auxiliary variables u_k, i.e. $N = 0$) is the linear one for passive-behaving dendrites. The voltage function reduces to $f_0(V) = V$ (resting potential set to zero) so the linear cable equations become

$$\frac{\partial}{\partial x}\left(\frac{1}{r_a(x)}\frac{\partial V}{\partial x}\right) = c(x)\frac{\partial V}{\partial t} + g(x)V \tag{5}$$

2.1.2 Nonlinear cable

Hodgkin-Huxley model. Since the dendrites of many neurons may contain active ion channels in their membrane, the nonlinear cable equation has to be used for adequate modelling. Most of the realistic segment models are now based on the Hodgkin-Huxley (HH) voltage-dependent gate model.

In the original version, the model consists of a system of nonlinear differential equations ($N = 3$) for any neuronal segment (see Appendix A.1 for details).

FitzHugh-Nagumo model. Later in this paper we will use the FitzHugh-Nagumo (FHN) model, a simplified version ($N = 1$) of the Hodgkin-Huxley model with similar qualitative behaviour (see Appendix A.2 for details).

2.2 Transformation into normal form

To remove the various specific constants we transform (3) by the variable transformation (Schierwagen 1989, 1994)

$$T = \frac{t}{\tau} \qquad \text{with} \quad \tau(x) = \frac{c(x)}{g(x)} \tag{6a}$$

and

$$X = \int_0^x \frac{\mathrm{d}\hat{x}}{\lambda(\hat{x})} \qquad \text{with} \quad \lambda(x) = \frac{1}{\sqrt{r_a(x)g(x)}} \tag{6b}$$

All quantities expressed in these dimensionless coordinates are referred to as electrotonic quantities, e.g. the electrotonic length L of a segment is defined by $L = \int_0^x 1/\lambda(s)\mathrm{d}s$. For a uniform cable, i.e. c, g and r_a independent of x, λ and τ are constant and equal to the length and time constants of passive cable theory.

Now (3) can be rewritten:

$$0 = \frac{\partial^2 V}{\partial X^2} + Q\frac{\partial V}{\partial X} - \frac{\partial V}{\partial T} - f_0(X, V, u_1, \ldots, u_N) \tag{7a}$$

$$\frac{\partial u_k}{\partial T} = \tau f_k(X, V, u_1, \ldots, u_N) \quad \text{for } 1 \le k \le N \tag{7b}$$

with

$$Q(X) = \frac{1}{2}\frac{d}{dX}\ln\left(\frac{g(X)}{r_a(X)}\right) \tag{7c}$$

$Q(X)$ contains all geometry-dependent parts of the transformed cable equation and can therefore be used for classifying cable geometries. For example, in the standard case of a cable with circular cross-section, Q results in

$$Q(X) \overset{(4)}{=} \frac{d}{dX}\ln\left(d(X)^{\frac{3}{2}}\sqrt[4]{1 + \frac{1}{4}\left(\frac{dd}{dx}\right)^2}\right)$$

In particular, we get $Q = 0$ for all cylindrical cable geometries (i.e. r_a and g are constant), whereas Q remains nearly constant for a (slowly) exponential tapering segment-diameter in (4) – positive for increasing and negative for decreasing diameter. Further useful geometry types for analytical treatment can be found in Schierwagen (1989). In the following, however, $Q(X)$ will be considered as a free parameter.

The axial current j_a [see (1)] transformed into the normalized coordinate system is then given by

$$j_a(X, T) = -\sqrt{\frac{g(X)}{r_a(X)}}\frac{\partial V}{\partial X} \tag{8}$$

3 Representation of a neuronal tree

To represent a neuronal tree, we use the graph-theoretical concept of a directed, labelled tree. All branching points of the dendrite are then represented by the nodes of the tree with the soma as root point. By means of additional (virtual) nodes, various functional aspects can be described (e.g. synaptic input into a segment, 'hot spots' on segments, the soma attached to

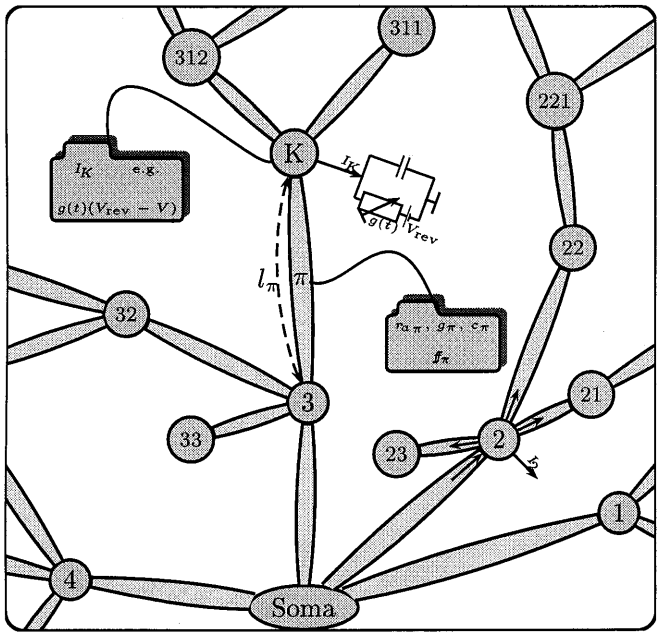

Fig. 3. Tree representation of a neuronal structure. Edges are labelled with electrical properties of the represented segment, e.g. functions of axial and membrane resistance/capacitance. Nodes are labelled by point-like current functions, e.g. synaptic input.

the root of the tree). The edges of the tree correspond to single neuronal (sub-)segments. All tree elements (nodes, edges) are labelled by their electrical properties.

3.1 Edge and node labels

Any edge $\pi = (K, L)$ from node K to node L is labelled with the quantities necessary to set up the cable equation for the corresponding cable segment, i.e. length l_π, number N_π of auxiliary variables u_k, functions $r_{a\pi}$, g_π, c_π, f_π and $f_{\pi k}$, describing the electrical behaviour of the segment (Fig. 3). Note that the origin of the space variables x and X is the root node.

In addition to their topological meaning as branching points, the nodes of a tree are useful for incorporating additional point-like currents as stated above. To model this, every node K has to be labelled with a current function $I_K = I_K(t, V, \partial V/\partial t)$ that depends on the voltage and its time derivative at this site, and explicitly from time. Examples are synaptic input modelled by a change of synaptic conductance

$$I_K = \begin{cases} 0 & \text{if } t \le \Delta \\ -\frac{g_{\max}\tau}{\mathrm{e}}(t-\Delta)\exp\left(\frac{\Delta - t}{\tau}\right)(V_{\text{rev}} - V) & \text{if } t > \Delta \end{cases}$$

and a lumped soma or boundary conditions at the tips modelled by an RC circuit

$$I_K = \frac{1}{R_K} V + C_K \frac{\partial V}{\partial t}$$

A more complicated example is a localized hot spot described by a nonlinear current function, e.g.

$$I_K = \frac{1}{R_K} V \left(1 - \frac{V}{V_1}\right)\left(1 - \frac{V}{V_2}\right)$$

with an amplifying range $[V_1, V_2]$ as in the FHN model. To achieve more realistic models it is also possible to use additional auxiliary variables with further defining differential equations analogously to the nonlinear cable equation. But here all variables have to be independent of the space coordinate (otherwise such hot spots should be modelled by dividing the segment containing them into subsegments described by different cable equations, e.g. alternating passive and active cables). Therefore, hot spots can be described by the localized HH equations (A.1).

3.2 Boundary conditions

The recursive structure of a tree can be used to define the following functions on nodes and edges:

Definition 1. *$\mathscr{CS}(K)$ denotes the set of all child segments with K as the starting node.*

$\mathscr{PS}(K)$ stands for the (unique) parent segment with K as the end node.

X_L is the electrotonic distance of the node L from the soma, i.e. $X_S = 0$ and for all segments $\pi = (K,L)$ holds $X_L = X_K + L_\pi$ (with L_π as the electrotonic length of π).

With the introduced notation we can combine all the current and voltage equations for single segments (7) by their boundary conditions at the nodes. From Kirchhoff's first law, we get

$$j_{a\mathscr{PS}(K)}(X_K, t) = I_K + \sum_{\pi \in \mathscr{CS}(K)} j_{a\pi}(X_K, t) \tag{9}$$

To determine the voltage and current distribution over a given neuronal tree resulting from some external input described by current functions I_K we have to solve (7) for all segments on the above boundary conditions (9).

3.3 Example of neuronal tree representation

An example of the neuronal tree representation introduced above is given in Fig. 3. The soma S of the neuronal structure has four child nodes[2] $K_1, \ldots, K_4$ connected by the main segments $(S, K_1), \ldots, (S, K_4)$. From these nodes further branching points can be reached, e.g. node K_{33} by segment (K_3, K_{33}).

For example, the set $\mathscr{CS}(K_2)$ of child segments of node K_2 (corresponding to Fig. 3) then reads:

$$\mathscr{CS}(K_2) = \{(K_2, K_{21}), (K_2, K_{22}), (K_2, K_{23})\} \tag{10}$$

and the parent segment of K_{32}

$$\mathscr{PS}K_{32} = (K_3, K_{32}) \tag{11}$$

[2] For simplicity, in formulae and in figures nodes are denoted by their indices.

Therefore, the boundary condition (9) at node K_2 results in

$$j_{a(S,2)}(X_S,t) = I_2 + j_{a(2,21)}(X_2,t) + j_{a(2,22)}(X_2,t) + j_{a(2,23)}(X_2,t)$$

where $j_{a(S,2)}$ is the axial current flowing from segment $(S,2)$ into node K_2, and $j_{a(2,21)} \ldots j_{a(2,23)}$ are the axial currents entering the corresponding segment from node 2 (cf. the arrows to and from node K_2 in Fig. 3).

4 Equivalent cable model of a neuronal tree with active membrane

Obviously, the problem of finding the voltage distribution over a given neuronal tree is hard to solve in general. In most cases the only way to gain some insight into possible reactions of the system lies in numerical simulations, which often remain unsatisfactory because of the great complexity of such systems (thousands of segments and ten thousands of synapses for realistically modelled trees). Thus, any reduction of the original problem to one with fewer system parameters would be of great help.

We will show here that the reduction approach derived for passive dendrites (Rall 1962; Schierwagen 1989) can be generalized in two ways: neuronal trees with active membranes can be reduced to an equivalent non-uniform cable, or a greater variety of morphologically defined tree classes can be collapsed to a single cable.

After stating the main result in strictly technical notions we will explain it in more qualitative terms.

4.1 Main theorem

Definition 2 (equivalent cable). *We define a (finite) cable to be equivalent to a given neuronal tree under specific boundary conditions (current and/or voltage input) if there exists an injective mapping T_{eq} from the neuronal tree to the equivalent cable with the following properties:*

- *T_{eq} is bijective on any path [i.e. on all segments between the root (soma) and a leaf (tip)] through the neuron;*
- *the voltage change with time at any point X_π in the tree is equal to the voltage change of the equivalent cable at point $Y = T_{\mathrm{eq}}(X_\pi)$:*

$$\forall T \geq 0 \colon V_\pi(X_\pi, T) = V(Y,T)^i \tag{12}$$

- *the sum of axial current flowing through all segments at points X_π with the same image $Y = T_{\mathrm{eq}}(X_\pi)$ (i.e. of points X_π which are equivalent relative to the map T_{eq}) equals the axial current of the equivalent cable at Y:*

$$\sum_{\pi=(K,L)\mid Y\in(X_K,X_L]} j_{a\pi}(Y,T) = j_{a_{\mathrm{eq}}}(X_\pi,T) \tag{13}$$

This means that every solution (voltage and current distribution) for such an equivalent cable leads straight to a solution for the whole tree by means of the mapping T_{eq}.

If we choose the map T_{eq} as the projection map (mapping X_π at segment π with electrotonic distance X from the soma to X on the equivalent cable) we can find sufficient conditions for reducing trees to an equivalent cable. With the equivalent cable described by the cable equation (7) with parameters l_{eq}, $r_{a_{\mathrm{eq}}}$, g_{eq}, c_{eq}, n_{eq}, f_{eq} and f_{eq_k} the conditions are the following:

1. For all segments π, π' time constants have to be *really* constant and independent of the segments ($\tau_\pi = \tau'_\pi$). We define the time constant of the equivalent cable as $\tau_{\mathrm{eq}} = \tau_\pi$.[3]
2. All terminal nodes T have the same electrotonic distance L_T from the root S:

$$L_T = X_T = \int_0^{X_T} \frac{dx}{\lambda(x_\pi)} = L_{\mathrm{eq}}$$

3. The voltage functions $f_{\pi i}$ ($i \in \{0,1,\ldots,N\}$) are equal in all parallel segment domains $[X_1, X_2]$ (the grey-labelled regions in the example of Fig. 4), i.e. for all $X \in [X_1, X_2]$:

$$f_{\pi_i}(X_\pi, V, u_1, \ldots, u_N) = f_{\mathrm{eq}_i}(X, V, u_1, \ldots, u_N) \ .$$

4. All segments are of the same geometric type, i.e. for any segment π the geometrical parameter Q_π equals the geometrical parameter of the equivalent cable in the corresponding X domain, $Q_\pi(X_\pi) = Q_{\mathrm{eq}}(X)$. Using (7c) it follows that there are (integration) constants B_π for any segment π with

$$\sqrt{\frac{g_\pi(X_\pi)}{r_{a\pi}(X_\pi)}} = B_\pi \sqrt{\frac{g_{\mathrm{eq}}(X)}{r_{a_{\mathrm{eq}}}(X)}} \tag{14}$$

Furthermore, at the nodes of the tree an additional condition must be satisfied: the constant B_π belonging to a parent segment π (with $B_{\mathscr{P}\mathscr{S}S} := 1$ for the nonexistent parent segment of the root) has to equal the sum of the B'_π which belong to all child segments π' of π:

$$B_\pi = \sum_{\pi' \in \mathscr{C}\mathscr{S}(\pi)} B'_\pi \tag{15}$$

5. All (non-vanishing) current functions I_K at nodes K have to be divided among all locations at the same electrotonic distance from the root S corresponding to the weights of their parent segments $B_{\mathscr{P}\mathscr{S}(K)}$, that is, any two nodes K and L with $X_K = X_L$ have to satisfy

$$I_K / B_{\mathscr{P}\mathscr{S}(K)} = I_L / B_{\mathscr{P}\mathscr{S}(L)} \tag{16}$$

[3] It would be possible to get an equivalent cable also for varying τ, but this would complicate the procedure because the time transformation (6a) could not be done. Moreover, some of the following conditions would contain explicitly τ, which does not seem very realistic.

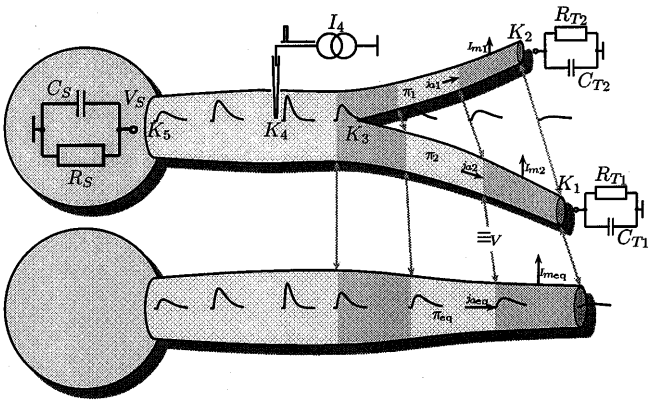

Fig. 4. A simple neuronal tree and its 'equivalent cable'. A current input $I_4(t)$ is injected into the main segment (defining the node K_4) of the tree with only one branching point (K_3). The soma (K_5) and both segment terminations (K_1 and K_2) are modelled by simple *RC* components. I_3 vanishes in this example. The equivalent cable is constructed in such a way that there is an injective mapping T_{eq} from the tree to the equivalent cable that connects 'equivalent' ($\equiv_V$) sites. For the first segment in this example this is obvious because there is only one. In the remaining part *grey double arrows* refer to sites with identical voltage changes according to the equivalent cable model derived. Additionally, the *grey-labelled regions* between equivalent points have the same total current flow in the axial direction ($j_{a1} + j_{a2} = j_{a\text{eq}}$) and across the membrane ($I_{m1} + I_{m2} = I_{m_{\text{eq}}}$)

Then the current function I_X^{eq} into the equivalent cable at the same electrotonic distance $X = X_K$ is defined by the sum of all inputs at equal electrotonic distance X:

$$I_X^{\text{eq}} := \sum_{X_L = X} I_L \tag{17}$$

We can now state the main result of this paper:

Theorem 1 (equivalent cable). *For any neuronal tree fulfilling the above conditions, an equivalent cable can be constructed by means of (14) and (17).*

An outline of the proof is given in Appendix B.

4.2 Special case of equivalent cylinder

For a better understanding of the above conditions it may be helpful to look for examples of trees satisfying them. For instance, the well-known equivalent cylinder model for passive dendrites (Rall 1962) can be derived as a special case. To see this we will compare all our conditions with Rall's:

1. In Rall's model of an equivalent cylinder all specific cell parameters R_i, R_m and C_m are assumed to be constant over the whole tree, i.e. τ is constant too.
2. The second condition is identical to Rall's.
3. In Rall's model there is only one voltage function, $f_0(X) = V$ (the linear case), which makes the third condition trivial.
4. In the case of a tree with cylindrical segments, i.e. $g_\pi(X)/r_{a\pi}(X) \sim d_\pi^3$ and $Q(X) = 0$, and constant specific cell parameters R_i, R_m and C_m our generalized branching condition (15) reduces to Rall's 3/2 branching rule, because (14) reads then [with $\sqrt{g_\pi(X)/r_{a\pi}(X)} \sim d_\pi^{\frac{3}{2}}$ for uniform segments] $B_\pi = (d_\pi/d_{\text{eq}})^{\frac{3}{2}}$, giving for (15):

$$d_\pi^{\frac{3}{2}} = \sum_{\pi' \in \mathscr{G}\mathscr{S}(\pi)} d_{\pi'}^{\frac{3}{2}} \tag{18}$$

5. In Rall's model there is an analogue for the boundary conditions at the tips (covered here under the general current functions I_K to node K) that have to be either zero or all equal in the totally symmetrical branching tree, which is clearly a special case of our fifth condition. Current injection into the symmetrical tree is also assumed to be divided symmetrically among all sites at an equal electrotonic distance from the soma.

Corollary 1. *If compared with Rall's equivalent cylinder model, the class of neuronal trees allowing the reduction to an equivalent cable is enlarged by new geometric types (see Fig. 5) and membranes with active ion channels.*[4]

4.3 Explanation of the tree reduction concept

In this section, the simple neuronal tree displayed in Fig. 4 will be used to exemplify the equivalent cable definition and the reduction process. The tree starts with a single main segment branching into two child segments π_1 and π_2 of different length and diameter. All segments are assumed to have a circular cross-section corresponding to Sect. 2.1 with a homogeneous distribution of ion channels so that the voltage functions $f_{\pi i}$ are independent of the space variable. The question then is under which conditions the child segments can be reduced to a single (sub-)cable with equivalent (in a certain sense) electrical behaviour. This would lead to a representation of the tree by only one segment (with in general non-uniform diameter and an additional discontinuity at the former branching point).

4.3.1 The concept of equivalence between neuronal tree and cable. First we have to clarify the meaning of 'equivalent electrical behaviour', i.e. what led us to Definition 2.

Taking the reduction process verbatim, the following question arises: Is it possible to get a single segment by 'cutting open' both child segments π_1 and π_2 and subsequently 'sticking them together', so that with the corresponding boundary conditions (in the example a

[4] We should note here that for passive trees there are efficient methods to analyse the full tree structure directly so that the concept of an equivalent cable is no longer of importance in this case. (van Pelt 1992; Agmon-Snir and Segev 1993; Ohme and Schierwagen 1996a).

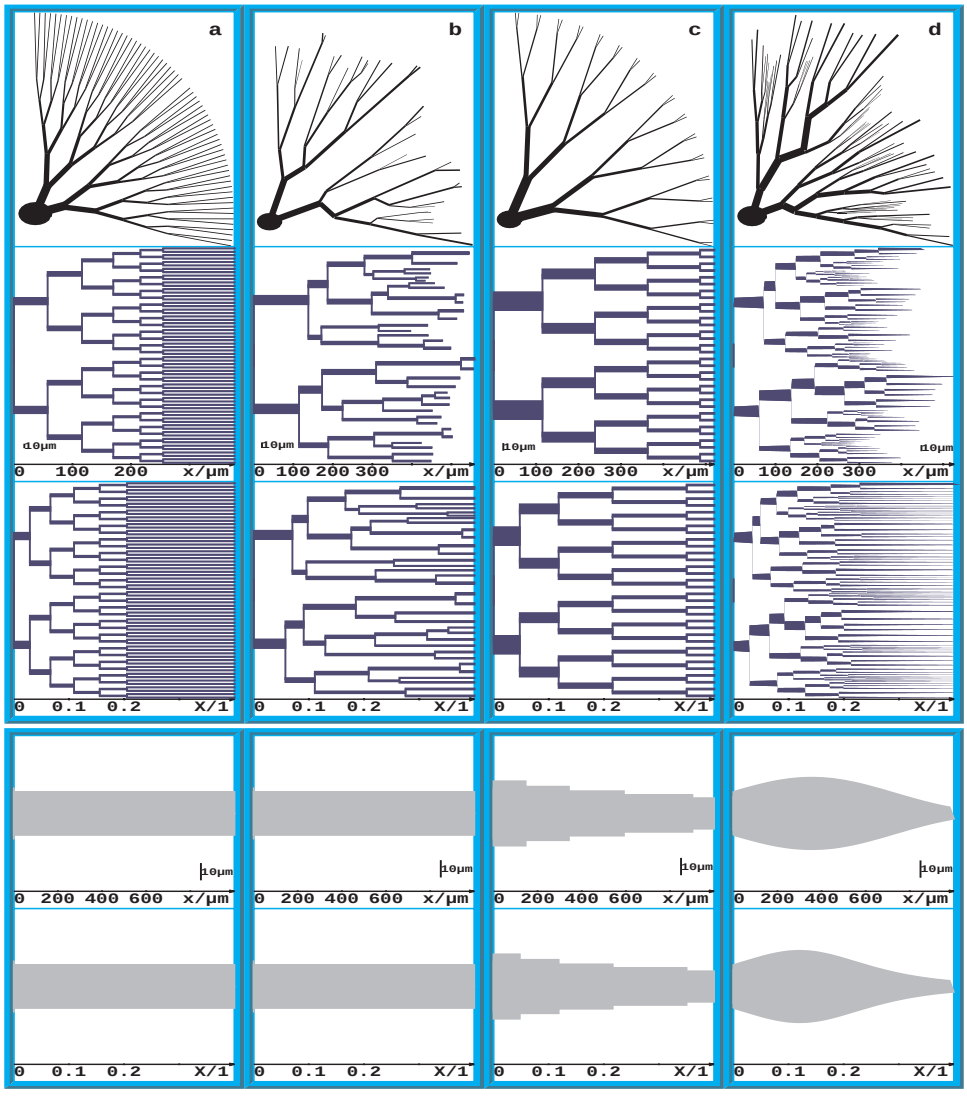

Fig. 5a–d. Some theoretical trees and their equivalent cables. Every column should be read from top to bottom: the original tree, its dendrogram in physical x- and normalized X-space and its equivalent cable in physical x- and normalized X-space. The following tree types are displayed: **a** a symmetrical branching tree that collapses into one equivalent cylinder, **b** an asymmetrical tree also collapsing into one equivalent cylinder, **c** a symmetrical branching tree failing Rall's 3/2 branching rule and therefore reducing to a non-continuous cable, and **d** an asymmetrical tree reducing to a non-uniform (sinusoidal) equivalent cable

current injected in node K_4) the same voltage and current distributions result in the now merged and henceforth everywhere electrically connected segments? The basic premise is that no additional current is introduced between the previously separate cable segments. That means that only points with equal voltage transients in the branched model should be 'stuck together' (demonstrated in Fig. 4 by the equivalence relation $\equiv_V$), which prevents the initiation of voltage gradients over the 'sticking area'. Therefore, we have to introduce a transformation (the mapping T_{eq} in Definition 2 and in Theorem 1) for scaling the child segments before the 'sticking process' can be carried out.

4.3.2 Choosing the transformation. Having specified such a mapping T_{eq} (and the induced equivalence relation between the branched subtree and the 'stuck' equivalent cable) the voltage distribution on the subtree can easily be deduced from the voltage distribution on its equivalent cable. Finding this mapping, however, requires prior knowledge of the voltage solution. To overcome this 'bootstrapping problem' we choose the normalization or electrotonic transformation according to (6). This allows us to check simply the additional conditions for the neuronal tree to admit exactly this special map. Additionally, it has the special property of being valid for a large class of boundary conditions for the tree, at least for all kinds of somatic current injections and voltage clamps – i.e. despite different resulting voltage distributions, the equivalence relation $\equiv_V$ remains unchanged.

This becomes clearer if we look at the normalized cable equation for the child segments π_1 and π_2 to be joined. They are identical (and have therefore the same set of solutions) if firstly τ and f_π in (7b) depend on X in the same way. This is guaranteed by Conditions 1 and 3. Secondly, (7a) becomes identical for both segments if also $Q_{\pi_1}(X) = Q_{\pi_2}(X)$ as expressed in the first part of Condition 4. This means that the geometrical shape for 'parallel' segment parts (with their boundary at equivalent points in each case: see grey-labelled regions in Fig. 4) have to be similar, i.e. their diameter functions have all to be identical apart from a scaling constant (B_π). This results from deriving the logarithm of the

diameter function in the definition of Q in (7c): see (14) of Condition 4 of Theorem 1. For cylindrical segments, for instance, this is always fulfilled because of $Q = 0$, which means, however, that for neuronal trees with cylindrical segments, the equivalent cable will always be composed of cylindrical parts.

However, additional conditions are necessary to guarantee that for each segment the same special voltage solutions also arise from the equal set of general ones. For instance, the sum of the currents flowing into two child segments has to equal the current flowing into the 'fused' equivalent cable (see arrows into and out of the grey-labelled regions in Fig. 4). If we recursively calculate this for the whole neuronal tree, we get the second (15) of Condition 4 of Theorem 1 by means of (8) for the axial current and the similarity relation (14). In addition, all tips have to be at the same electrotonic distance from the soma (Condition 2), and external input must not disturb this current/voltage equilibrium (Condition 5).

5 Practical aspects of the reduction process

5.1 Construction of the equivalent cable

In most cases reconstructed neuronal trees will not strictly meet the conditions for reduction. So we are in need of an algorithm that maps a tree onto a 'nearly' equivalent cable. One approximation method often used in numerical mathematics is to ensure that the algorithm gives the correct results for the subclass of arguments where the correct solution is known. This means in our case that the algorithm should result in the correct equivalent cable for all trees that fulfil our conditions for reduction.

For the subclass of trees satisfying Conditions 1 and 3 (e.g. with homogeneously distributed ion channels) we can construct such an 'approximately equivalent cable' according to

$$\sqrt{\frac{g_{\mathrm{appr}}(X)}{r_{a\mathrm{appr}}(X)}} = \sum_{\pi=(K,L)|X\in(X_K,X_L]} \sqrt{\frac{g_\pi(X)}{r_{a\pi}(X)}} \tag{19}$$

Note that the cable defined by (19) is ambiguous because only the quotient $g_{\mathrm{eq}}/r_{a_{\mathrm{eq}}}$ is determined. This works even for a cable with circular cross-section since (19) is then an ordinary differential equation without boundary conditions (see below).

The input currents to the cable defined by (19) should be set to the sum of all input currents in the tree at the same electrotonic distance from the soma [according to (16)]. Then it can be shown by induction (using especially Conditions 4 and 5) that the equivalent cable of any tree satisfying our reduction conditions equals the cable defined by (19) [and (16) for the input].

5.1.1 Special case of neuronal segments. If the segments of the neuronal tree and the equivalent cable are assumed to have circular cross-section the defining (19) reads [cf. (4)]:

$$d_{\mathrm{appr}}^{\frac{3}{2}}(X)\sqrt[4]{1+\frac{1}{4}\left(\frac{dd_{\mathrm{appr}}}{dx}\right)^2} = \sqrt{\sigma_{R_m}\sigma_{R_i}} \sum_{\pi=(K,L)|X\in(X_K,X_L]} d_\pi^{\frac{3}{2}}(X)\sqrt[4]{1+\frac{1}{4}\left(\frac{dd_\pi}{dx}\right)^2}$$

where $\sigma_{R_m} = R_{m_{\mathrm{appr}}}/R_m$ and $\sigma_{R_i} = R_{i_{\mathrm{appr}}}/R_i$ are scaling factors converting the specific electrical cell parameters R_m and R_i from the neuronal tree to the cable. To keep τ constant (cf. Condition 1 from Theorem 1) the specific membrane capacity has to be appropriately adapted: $C_{m_{\mathrm{appr}}} = C_m/\sigma_{R_m}$. Setting $\sigma_{R_m} = \sigma_{R_i} = 1$ keeps the specific cell parameters fixed.

For a neuronal tree with cylindrical cables we get

$$d_{\mathrm{appr}}^{\frac{3}{2}}(X) = \sqrt{\sigma_{R_m}\sigma_{R_i}} \sum_{\pi=(K,L)|X\in(X_K,X_L]} d_\pi^{\frac{3}{2}}(X) \tag{20}$$

because of zero diameter tapering ($dd/dx = 0$). In general, the resulting cable no longer results in a continuous cylinder.

5.1.2 Cartoon representation. In cases where the reconstructed neuronal tree has no equivalent cable and the cable defined by (19) does not approximate to the electrical behaviour of the cell a so-called cartoon representation of the cell should be used. Here only subtrees nearly fulfilling the reduction conditions are collapsed by means of (19) to a non-uniform cable – reducing the complex tree to a sparsely branched 'equivalent tree' (Stratford et al. 1989).

5.2. Comparison of two usual reduction methods in view of our theoretical results

In the previous section we developed a method to reduce neuronal trees to a single cable that will result in a nearly equivalent cable for some trees. There are other methods with the same aim, however, without firm theoretical basis. We will compare here two of them that are often used.

Both methods define morphological invariants that the reduction process has to preserve: the total cross-sectional area (Bush and Sejnowski 1993) and the total membrane area in the construction of the 'equivalent dendritic profile' (Clements and Redman 1989), respectively. Both invariants are in relation to the electrical behaviour – the cross-sectional area to the axial current and the total membrane area to the membrane current. However, keeping one area fixed does not mean that the related electrical quantities remain fixed as well. Thus, the question is which of these reduction methods may be better in terms of electrical equivalence.

5.2.1 Conservation of cross-sectional area. The cross-sectional area of the tree can be kept fixed if the diameter $d_\emptyset$ of the constructed cable is defined by:

$$d_\emptyset^2(x) = \sum_{\pi=(K,L)|x\in(x_K,x_L]} d_\pi^2(x) \tag{21}$$

i.e. the summation over the segments is done in the original rather than in the electrotonic space, simplifying the reduction process compared with (20). A further advantage is the comparable length dimension of the cable thus constructed with the original tree: the length of the cable is not larger than any path from the soma to a tip in the original tree, whereas the equivalent cable is generally longer.

However, to achieve a satisfactory approximation of the electrical behaviour the R_m and C_m values assigned to the reduced cable have to be adapted with a subsequent optimization procedure (Bush and Sejnowski 1993). Even for trees that possess an electrical equivalent cable in the sense of Definition 2, this may lead to a rather weak approximation requiring the use of a cartoon representation of the cell. The reason is that the total axial current at x only remains equal for both the cable according to (21) and the tree if the voltage at x is also invariant. On the other hand, the voltage distribution depends crucially on the total membrane current at x, which requires [for an assumed invariant voltage $V(x) = V_\emptyset(x)$ we have to compare the cable perimeters]:

$$d_\emptyset(x) = \sum_{\pi=(K,L)|x\in(x_K,x_L]} d_\pi(x)$$

which contradicts (21).

5.2.2 Dendritic profile. The total membrane area remains fixed during the reduction process if the diameter d_{prof} of the reduced cable is defined by (Clements and Redman 1989)

$$d_{\text{prof}}^{\frac{3}{2}}(X) = \sum_{\pi=(K,L)|X\in(X_K,X_L]} d_\pi^{\frac{3}{2}}(X) \tag{22}$$

where X is the electrotonic distance from the soma. This yields for any subdomain $[X_1, X_2]$ of the cable and the tree.

A drawback of this method lies in the additional computational cost of the electrotonic transformation. Also, the length of the dendritic profile after back-transformation into x-space is – at least for complex branched trees – much larger than the largest distance in the original tree, allowing conclusions based on spatial relations (for instance for layered synaptic input) only by roundabout means of the electrotonic transformation.

It has been shown empirically, however, that this reduction leads to satisfactory approximations of input resistance R_{in} and of the first time constant τ_0 with its coefficient C_0 in voltage transients – without optimizing any of the specific electrical parameters R_m, R_i or C_m (Holmes and Rall 1992). Additionally, comparing (22) with (20) for $\sigma_{R_m} = \sigma_{R_i} = 1$ we find that the dendritic profile turns out to be a special case of our equivalent cable concept. So at least for trees fulfilling the equivalent cable conditions, the dendritic profile constructed according to (22) with the same specific electrical parameters and ion channel distribution and appropriate input conditions is electrically equivalent in the sense of Definition 2. Therefore, for these trees both the total axial and membrane current remain invariant (measured at electrotonic distances) during the reduction process.

5.3 Equivalent cable model retaining length

We have seen above that the effort of keeping morphological parameters constant during the reduction process may conflict with the aim of constructing a cable with approximate electrically equivalent behaviour. In the following we show a way to preserve at least the mean length from soma to the tips (for symmetrical branching trees one reaches even equality) while getting the electrical equivalent cable in the sense of Definition 2 in case it exists. This is especially useful for analysing the effect of layered input by means of the equivalent cable (cf. Fig. 1).

For this we use the construction equations (20) for trees with cylindrical segments. As in Bush and Sejnowski (1993) an additional adaptation of the specific cell parameters $R_{m_{\text{red}}}$ and $C_{m_{\text{red}}}$ of the reduced cable is necessary, however, without an additional optimization process. With $\sigma_{R_m} = R_{m_{\text{red}}}/R_m$ as the scaling factor for the adaptation of the specific membrane resistance (and with $C_{m_{\text{red}}} = C_m/\sigma_{R_m}$) the construction equation for the 'scaled dendritic profile' reads [cf. (20) with $\sigma_{R_i} = 1$]:

$$d_{\text{red}}^{\frac{3}{2}}(X) = \sqrt{\sigma_{R_m}} \sum_{\pi=(K,L)|X\in(X_K,X_L]} d_\pi^{\frac{3}{2}}(X) = \sqrt{\sigma_{R_m}}\, d_{\text{prof}}^{\frac{3}{2}}(X)$$

Transforming this back into the original space by inverting the normalization transformation, (6b), we get

$$\begin{aligned} x &= \sqrt{\frac{R_{m_{\text{red}}}}{4R_{i_{\text{red}}}}} \int_0^X \sqrt{d_{\text{red}}(\hat{X})}\,\mathrm{d}\hat{X} \\ &= \sigma_{R_m}^{\frac{2}{3}} \left(\sqrt{\frac{R_m}{4R_i}} \int_0^X \sqrt{d_{\text{prof}}(\hat{X})}\,\mathrm{d}\hat{X} \right) \end{aligned}$$

i.e.

$$d_{\text{red}}^{\frac{3}{2}}(x) = \sqrt{\sigma_{R_m}}\, d_{\text{prof}}^{\frac{3}{2}} \left(\frac{x}{\sigma_{R_m}^{\frac{2}{3}}} \right)$$

With an appropriate small scaling factor σ_{R_m} the length of the cable $l_{\text{red}} = \sigma_{R_m} l_{\text{prof}}$ can be adapted to the mean length of the original neuronal tree. Additionally, we get a decrease in its diameter, so that the mean total cross-sectional area is approximately preserved.

If the two parameters length and cross-sectional area are adapted independently of each other the specific intracellular membrane resistance has to be scaled as well ($\sigma_{R_i} = R_{i_{\text{red}}}/R_i$):

$$d_{\text{red}}^{\frac{3}{2}}(x) = \sqrt{\sigma_{R_m}\sigma_{R_i}}\, d_{\text{prof}}^{\frac{3}{2}} \left(\frac{\sigma_{R_i}^{\frac{1}{3}}}{\sigma_{R_m}^{\frac{2}{3}}} x \right) \tag{23}$$

For this method all calculations have to be done in the normalized space, making it computationally more expensive than the method of Bush and Sejnowski

(1993). On the other hand, it preserves the good electrical approximation features of the dendritic profile, saving additional optimizations, and the demand for an equivalent cable with comparable length can be satisfied.

6 Example: equivalent cable models of two neuronal trees

To illustrate the application of our approach we studied the signal flow in two neuronal trees and their dendritic profiles. One tree (the 'ideal' neuron) fulfils our reduction criteria whereas the other (the 'non-ideal' neuron) violates some of them, leading, nevertheless, to appropriate results.

We studied four different input scenarios: active membrane against passive, and somatic input against dendritic. Because of the assumed nonlinearity of the membrane the analysis of the reduced cables is done by compartmental simulation, i.e. by discretization of the underlying differential equations in space and time. In general, the advantage of the reduced model lies in the decrease in the number of resulting equations.

6.1 Simulation methods

Simulations were performed using our program DENDRIT (Ohme and Schierwagen 1994) for computer-assisted morphological analysis. It allowed us to analyse neuronal trees and to generate approximate equivalent cables. Here, we also used the reverse ability for creating an equivalent tree to a given single cable.

The numerical calculations were carried out by the simulation program SPICE (Segev et al. 1985; Bunow et al. 1985), for which DENDRIT generates a circuit description file from the neuronal tree by compartmental decomposition.

6.2 Model parameters

All segments are described by the FitzHugh-Nagumo system (see Appendix A.2 for details), which has one ($N = 1$) auxiliary variable u and a cubic current-voltage relation f in (3).

The electrical parameters r_a, g and c result from the standard equations for a non-uniform cable of circular

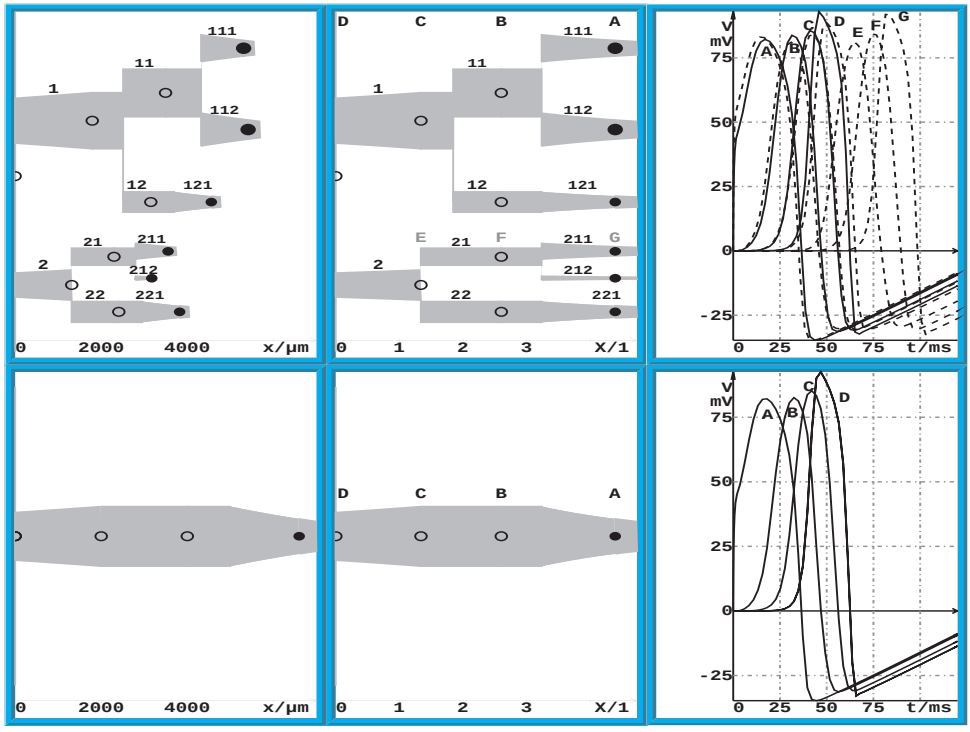

Fig. 6. Comparison of active excitation propagation in a branched neuronal structure (*top*) and in the corresponding equivalent cable (*bottom*). For each case is shown (a) the tree as a dendrogram in the original (*left*) and (b) in the normalized space (*middle*) and (c) the results of the simulation (*right*). The segments of the tree are of different geometric type, from soma to tips firstly with increasing ($Q = 0.09$), then with uniform ($Q = 0$) and eventually with decreasing ($Q = -0.26$) diameter. We assumed a uniform distribution of active ion channels over the tree modelled by the FitzHugh-Nagumo system ($R_i = 200\,\Omega\,\mathrm{cm}^2$, $R_m = 20\,000\,\Omega\,\mathrm{cm}$, $C_m = 1\,\mu\mathrm{F/cm}$, $V_1 = 5\,\mathrm{mV}$, $V_2 = 100\,\mathrm{mV}$, $\alpha = 2 \times 10^{-7}\,\mathrm{s}^{-1}$ and $\beta = 2 \times 10^{-9}\mathrm{s}^{-1}$). *Open circles* represent recording sites *B–D*, *filled circles* injection (and recording) sites *A* for the first simulation. In this case all conditions for the reduction of the dendritic tree to a single equivalent cable are fulfilled. The resulting voltage changes at the different recording sites are therefore identical (*continuous lines* in the simulation diagrams). In the case of a restricted input, into only two synapses (segments 111 and 112), the voltage responses are displayed (*dashed curves*). Note that differences of the voltage response at the recording sites increase with distance to the injection site. The second dendritic tree (with main dendrite 2) fulfils the conditions for representation as an equivalent cable, which makes the different voltage plots at equivalent recording sites (*F* as well as *G*) identical. See text for further details

cross-section [cf. (4)]. In the artificial neuron we used for demonstration purposes a fixed, slowly increasing (near the soma) or decreasing (at the terminals) exponential diameter function, i.e. $Q(X)$ in (7), is constant in all cases: positive for increasing, zero for uniform and negative for decreasing diameter. For the reconstructed neuron in Fig. 7 all segments were modelled as cylinders ($Q(X) = 0$).

Whereas the specific physiological constants correspond to values widely used in theoretical studies (Segev 1995) ($R_i = 200\ \Omega\,\mathrm{cm}^2$, $R_m = 20\,000\ \Omega\,\mathrm{cm}$ and $C_m = 1\ \mu\mathrm{F/cm}$) the dendritic lengths, strength of synaptic input and parameters of the FitzHugh-Nagumo model were chosen to admit a good visible travelling impulse solution.

6.3 Simulation results

6.3.1 Ideal neuron. Firstly, we consider a theoretical neuron with two dendritic trees connected through the soma (Fig. 6). Essential for the existence of an equivalent cable are (cf. Theorem 1):

- an equal electrotonic distance from the terminal nodes to the soma,
- an equal electrotonic distance from the synaptic inputs (filled circles in Fig. 6) to the soma, and
- correspondence of the equation types in equivalent X-domains [here only the segment geometry represented by $Q(X)$ changes whereas a uniform channel distribution is assumed – meaning that the f_k are independent of X over the whole tree].

Most of these requirements (except the homogeneous channel distribution) can be seen in the tree representation in normalized space (Fig. 6, second column).

The comparison of the whole neuronal tree and its equivalent cable showed the expected identity of simulation results. Thus, we will show in the following only a single example from the different runs – neuron and equivalent cable modelled with an active membrane and synaptic input into the dendrites according to the input condition of the equivalent cable (referred to as 'symmetrical' input). To demonstrate the influence of the correctly placed input, we tested it against a simulation with input concentrated at one place, therefore violating the equivalent cable conditions ('asymmetrical' input).

Symmetrical input. In the first simulation run the cell receives synaptic input (filled circles in the dendrogram) modelled by an α-shaped conductance change near the dendritic tips (segments 111, 112, 121, 211, 212 and 221) with strength proportional to $d^{\frac{3}{2}}$, i.e. the diameter at the corresponding site to the power $\frac{3}{2}$ [see (14) and (16)]. The 'recording sites' are the soma and some intermediate points (open circles in the dendrogram). In the top right-hand parts of Fig. 6 the resulting signals are shown. The continuous lines represent the voltage function at the recording sites (A corresponds to the input sites, D to the soma, B and C combine all the intermediate recording sites). The differences in the voltage functions at different recording sites at equal electrotonic distances from the soma are too small to be shown in the graph. The same is true for differences between the full tree (top) and the equivalent cable model (bottom).

Asymmetrical input. If we restrict the input to the cell to only two injection sites (synapses on segments 111 and 112) with the same total input current strength as in the equivalent cable, excitation propagation to the soma (dashed lines A, B, C and D) is similar to the first case, but at every branching point an impulse travels additionally backwards in the hitherto non-excited branches. This leads also to a small time delay for the somatic impulse. In Fig. 6 recording A corresponds to the voltage change at the injection sites (larger filled circles on segments 111 and 112), recordings B–E to responses at sites on segments 11, 1, soma and 2 (open circles). Recordings F and G denote the two and three coinciding responses at sites 21, 22 and 211, 212, 221. This is due to the property of the subtree emanating from segment 2 being reducible to an equivalent cable. Voltage responses from segments 12 and 121 are not shown here.

6.3.2 Neuron reconstructed from serial sections. In the second example we studied the reduction process for a reconstructed ('non-ideal') neuron violating some of the conditions for reducing it to an equivalent cable. Thus the terminals do not end at the same electrotonic length that can be seen in the lower left diagram of Fig. 7. However, the dendritic synapses are set according to the input condition of the equivalent cable and the cable is then constructed according to (20).

Local responses. Despite the violation of the reduction conditions the local responses of synaptic input are quite similar between the simulations of the full tree and of the dendritic profile (lines labelled S in Fig. 7) – even in the case of multiple synaptic input. This holds for both the linear and the FitzHugh-Nagumo model.

Remote responses. The results of the measurements at the remote (non-input) site (always labelled R in Fig. 7) differ more. They are, however, of comparable order of magnitude. Here it is remarkable that the results of one run with a simulated active membrane (seen in the rightmost diagram in Fig. 7 showing the active model with injection at the soma) are better approximated by the dendritic profile model than are the cases simulating a passive membrane. This might be based on the nearly bistable response behaviour (spike propagation) that appears only in this case.

These simulations suggest that the dendritic profile can lead to useful approximations of the response behaviour of the full cell even if the conditions of the reduction to an equivalent cable are not fulfilled.

7 Application: impact of neuronal tree type on spike (back-)propagation

As a first approach to the question of how dendrites of different geometrical type (Fig. 8) process input signals, we study here the effect of synaptic input into the terminals. In this situation the effect of geometrical type on signal propagation will be amplified. We are particu-

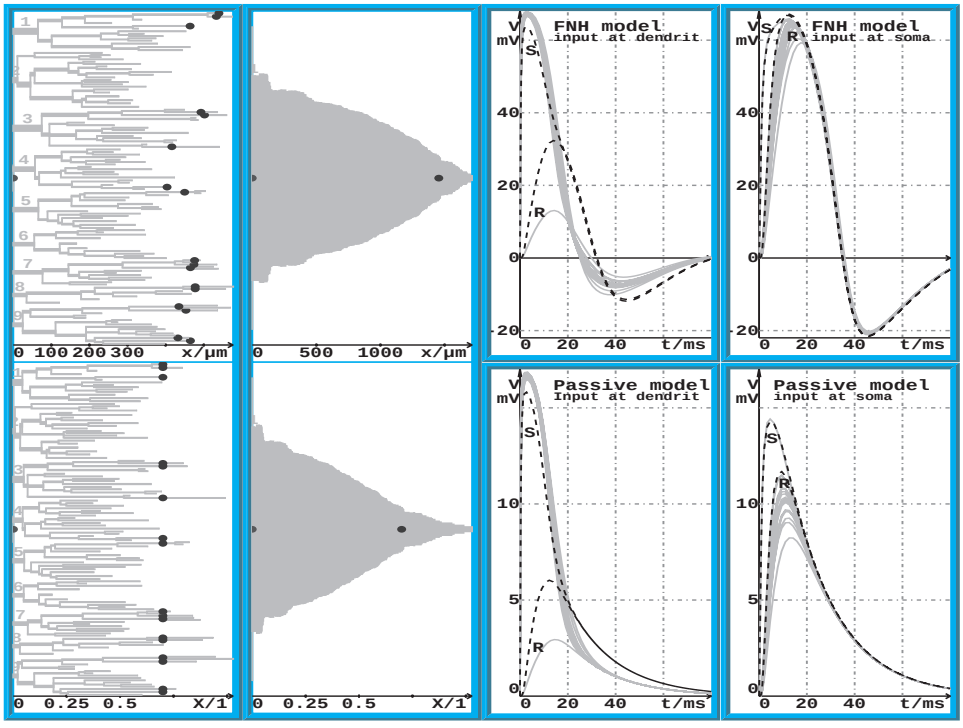

Fig. 7. Comparison of voltage spread in a reconstructed neuron of a cat deep superior colliculus neuron (Schierwagen and Grantyn 1986) (*left*) and in the corresponding dendritic profile (*second column*). They are shown in the original (*top*) and normalized space (*bottom*). The electrical parameters are taken from the previous example (see Fig. 6). Simulation results under different conditions are shown for the full tree (*continuous grey lines*) and the dendritic profile model (*dashed black lines*) in the diagrams of third and fourth column. They differ in the site of injection (*filled circles*) – at soma (*third column*) and at dendrites (*fourth column*) – and in the membrane properties – active FitzHugh-Nagumo model (*top*) and passive linear model (*bottom*). The total synaptic input to the dendritic tree is equal to the input to the soma according to (16). In all cases the voltage responses at the input site (labelled *S*) and the remote site (labelled *R*) are shown

larly interested in the capability of dendritic trees to carry spikes. Thus the dendrites are assumed to have continuously distributed active ion channels (modelled again by the FitzHugh-Nagumo system: see Appendix A.2).

7.1 Simulations with different tree types

One way to explore the response behaviour of different tree types is through numerical simulations of different input and membrane properties. Instead of simulating many single synaptic excitations in a fully branched dendrite, we reduce these trees to their equivalent cable (or a cable that matches it well) and sum all the synaptic input according to (17) into a single synaptic input at the end of the equivalent cable.

For this study we used three different cable geometries that were extracted from typical dendritic profiles found in real neurons (Fig. 8) by appropriately choosing the geometry parameter Q of (7c).

To measure only the impact of the geometric type we fixed all the electrophysical cell parameters, the length and normalized length of three different cables types (according to typical shapes seen in real neurons: Fig. 8) as well as the parameters of the synaptic input in our study.

We found (Fig. 9) that in case of orthodromic propagation only the uniform geometric type (top left) can propagate the spike along the cable, whereas the two other types, with a changing diameter (top middle and

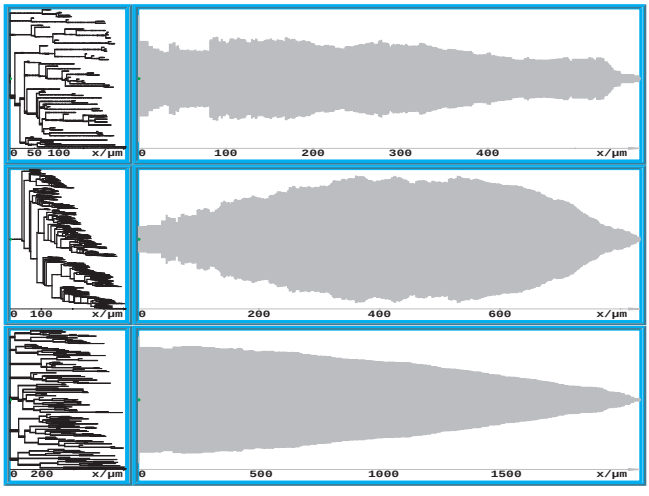

Fig. 8. Dendritic profiles of reconstructed neurons defining different equivalent cables. The dendritic profiles (as a first approximation to an equivalent cable) are shown. Whereas the upper cell (tectum neuron type T1 of a salamander; unpublished data of Roth, Dicke, Grunwald) approximates to an equivalent cylinder, the other two [guinea-pig cerebellar Purkinje cell (Rapp et al. 1994) (*middle*) and cat deep superior colliculus neuron (Schierwagen and Grantyn 1986) (*bottom*)] collapse to a non-uniform equivalent cable with trigonometrically (cos) changing and continuously decreasing diameter, respectively

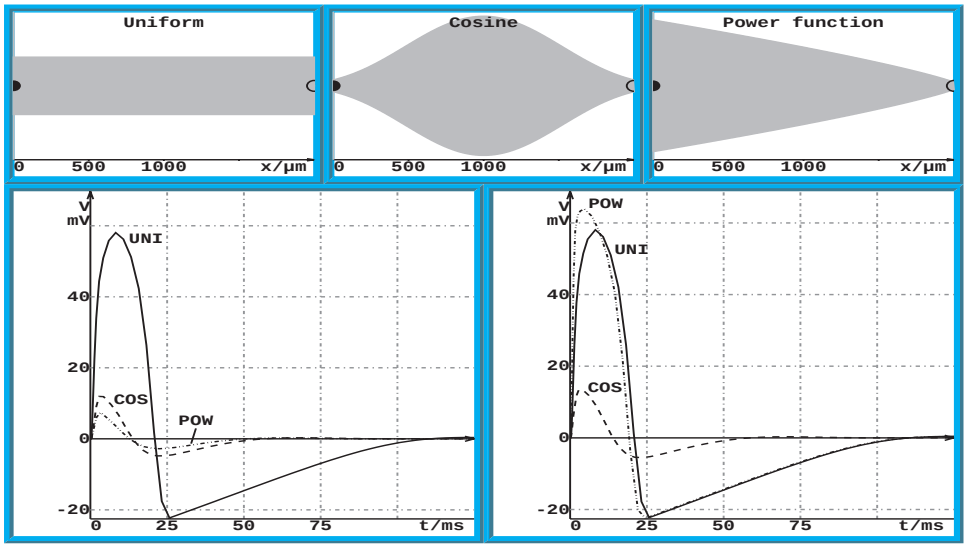

Fig. 9. Propagation of synaptic input (by a short α-shaped conductance change) from the tips (*right end*) of the equivalent cable to soma (*left end*) and vice versa. The voltage responses of three cables of different geometric type (*top*, from *left* to *right*: uniform, cosine and power profile) are shown in the *lower diagrams* [*left*: injection into the tips (*open circles*), *right*: injection into the soma (*filled circle*)]. The membrane is assumed to have active channels modelled by Fitz-Hugh-Nagumo equations

right), behave rather similarly to the lossy passive cable (simulation results are shown bottom left).

If we look instead for the antidromic propagation to the terminals of a spike generated near the soma then the uniform and declining cable types propagate the spike to the terminal tips but the trigonometrical type fails because of the initially increasing diameter profile (bottom right).

This qualitative behaviour remains relatively stable regardless of changes in synaptic input strength and shape as well as changes in the membrane parameter. Varying the impact of the soma (by changing its surface or specific electrical parameters), however, affects the excitation spread by the additional load similar to a change of the geometric type of the cable (increasing the soma surface is similar to widening the cable near the soma, increasing the chance for antidromic spikes against orthodromic).

Such contrasting behaviour — boosting antidromic spike propagation while failing to support dendritic spike initiation — has only recently been reported and analysed (Mainen et al. 1995; Stuart et al. 1997).

7.2 Theoretical considerations

If we look for a theoretical explanation of the different spike-propagation properties of the various geometrical tree types, a first hint comes from linear cable theory. Here it is well known that in a non-uniform cable, the voltage attenuation depends on the direction of signal spread: with decreasing diameter the attenuation is less than with increasing diameter. The asymmetry factor Ψ, defined as the quotient of the voltage attenuation in either direction, shows this exactly. For uniform cylinders with symmetrical boundary conditions it equals 1, but for monotonically changing diameter it computes to above or below 1, showing that the signal flows in the direction of decreasing cable diameter nearly undisturbed whereas it diminishes very fast in the opposite direction. In the case of a cable of trigonometrical type (with increasing and decreasing diameter) both signal directions are then strongly attenuating (for examples of voltage attenuation and Ψ values for different cable types see Schierwagen 1994).

In the case of active signal propagation, however, one could object to the explanation and simulations shown. It seems plausible to assume that a spike, once initiated, should travel further without change supported by the active ion channels, even in the direction with high electrical load.

However, this assumption does not hold in the present case of uniform density of active channels. To show this we consider travelling wave solutions of the normalized cable equations (7). Thus, we assume that in (7) only the geometry-defining parameter Q explicitly depends on the space variable X whereas all f_k are independent of X, i.e. the voltage thresholds of all channels do not vary in space. The same should hold for the auxiliary variables $u_k(X,T) = u_k(Y)$. Then we make the ansatz $V(X,T) = V(Y)$ with $Y = X - \Theta T$, which means that a fixed voltage shape travels (similar to the example in Fig. 6) with constant velocity Θ along the cable (for positive Θ from left to right). Now the system of ordinary differential equations to be solved reads

$$0 = \frac{d^2V}{dY^2} + (\Theta + Q)\frac{dV}{dY} - f_0(V, u_1, \ldots, u_N) \tag{24}$$

$$\frac{du_k}{dY} = -\frac{\tau}{\Theta} f_k(V, u_1, \ldots, u_N) \quad \text{for } 1 \le k \le N \tag{25}$$

For an uniform cylindrical cable, Q vanishes [see the definition of Q in (7c) with space-independent g and r_a]. Only in this case does (24) remain invariant with respect to the substitution $\Theta \to -\Theta$ and $Y \to -Y$, which means that for any leftwards travelling wave with velocity Θ^-, there is also a rightwards travelling wave with velocity $\Theta^+ = -\Theta^-$, and vice-versa.

For $Q > 0$ (the analogue is true for $Q < 0$) in some part of the segment under consideration this symmetry is broken – the range of possible wave velocities will be 'shifted'. For the general case of (24) no exact quantitative value of this shift can be given. We can explore it

qualitatively, however, by looking at the velocity of the leading wave-front. Assuming that the u_k kinetics are slower than the V kinetics, we let $u_k = 0$ during the build-up of the leading impulse front (Rinzel and Terman 1982). Equation (24) then reads

$$0 = \frac{d^2V}{dY^2} + (\Theta + Q)\frac{dV}{dY} - f_0(V) \tag{26}$$

Let the uniform cable equation with $Q = 0$ admit two travelling wave fronts (an excitation from the resting potential to some excited state) at a speed of Θ_{uni} – from right to left with $\Theta^- = -\Theta_{uni}$ and from left to right with $\Theta^+ = \Theta_{uni}$. Then the non-uniform cable admits two wave solutions with the shifted propagation velocities $\Theta^- = -(\Theta_{uni} + Q)$ and $\Theta^+ = \Theta_{uni} - Q$. For cable diameters increasing sufficiently strongly from left to right (high values of the geometry parameter Q) we find two wave solutions travelling to the left ($\Theta^- < \Theta^+ < 0$) but none travelling to the right. Here the left-travelling front also has a much higher speed than the fronts in the uniform cable.

These results demonstrate the direction-dependence of spike propagation in non-uniform cables (for deeper quantitative analysis see Schierwagen 1991; Ohme and Schierwagen 1993; Ohme 1996).

8 Evaluation of the reduction process

8.1 Numerical complexity

The concept of simplifying a neuronal tree to a single equivalent cable dramatically reduces the complexity of the problem that has to be solved. Take, for instance, a dendrite consisting of m single symmetrically branching trees with segments of branching order i $(1 \le i \le k)$ where the normalized lengths $L(i)$ of all segments of order i are equal. Then the number N_{tree} of compartments used by the numerical computation with the space discretization $\hat{L}$ would be

$$N_{tree} \ge m \sum_{i=1}^{k} 2^{i-1} \left\lceil \frac{L(i)}{\hat{L}} \right\rceil \overset{L(i)=L}{=} m(2^k - 1) \left\lceil \frac{L}{\hat{L}} \right\rceil$$

The number N_{eq} of compartments in which the equivalent cable splits under the same discretization conditions is

$$N_{eq} = \left\lceil \frac{\sum_{i=1}^{k} L(i)}{\hat{L}} \right\rceil \overset{L(i)=L}{=} \left\lceil k \frac{L}{\hat{L}} \right\rceil$$

i.e. the tree reduction yields an exponential diminution of the computational expenses in relation to the order k of the tree.

8.2 Analytical solutions

For some cases of equivalent cables even analytical solutions to active impulse propagation are available that cannot be deduced for the original branched trees. This can be achieved sometimes by a stepwise linearization of the nonlinearities in the cable differential equations of the equivalent cable, computing the general solution for all linear sub-domains and specifying the special solution by some continuation conditions at the domain boundaries. For the stepwise linearized Fitz-Hugh-Nagumo model travelling front (Schierwagen 1991) and travelling wave (Ohme 1996) solutions have been obtained for the uniform cylinder and some non-uniform cable geometries.

Another remark concerns the segment geometry. In Rall's original model all segments were assumed to be cylinders but the resulting equivalent cable could have varying diameter as well. For this the number $n(X)$ of segments has to vary continuously, which holds approximately only for very large trees. So at least two approximations are necessary: fitting dendritic segments by cylinders and then fitting the resulting stepwise linear diameter function by a continuous one. In this article we fitted only the segment shape by more general cable geometries and then obtained correct results for small numbers of dendritic branches as well.

In situations where this approach does not seem acceptable, one could stay with cylindrical segments and the resulting stepwise linear equivalent cable for which Theorem 1 holds, too.

8.3 Limitations of the method

Like any other reduction method, the present one also has its limitations. Obviously, only in exceptional cases will trees strictly meet the conditions for reduction. In the case of passive dendrites small deviations from these theoretical restrictions are tolerable, whereas in the active case this cannot be answered in general. If the solution for the equivalent cable is stable in the face of small changes in the model parameters (the length of the equivalent cable, the electrotonic parameters, input conditions and so on) the results obtained for the equivalent cable may be of use for the whole tree, too. This has to be shown in any case, however. As exemplified in the example in Sect. 6.3.2 nonlinear membrane properties may even lower the reduction error in some cases.

An obvious limitation of equivalent cable models is the loss of reduced spatial resolution. For instance, the equivalent cable preserves the distance of synaptic input from the soma, but no information about distances between synapses on different branches. So this method cannot address problems of local computation in dendrites. Thus, the main application field of the equivalent cable concept will be the analysis of massive layered input to the dendrites and excitation spread from the soma in the trees.

In both cases it may be possible to overcome these limitations by using an 'intermediate' reduction method, i.e. instead of collapsing the complex neuronal tree to a single cable, only parts of the tree should be simplified in accordance with the cartoon model in Stratford et al. (1989).

9 Conclusions

The aim of this study was to contribute to the problem of building reduced neuron models that allow the consideration of important functional properties such as spatially layered synaptic input. In the literature, equivalent cable models have been also employed for branched trees with active membrane, but without strict justification. As an example we mention Mel's clusteron model, which consists of a soma and a single dendritic segment. It has been shown that this model with Hebb-type learning rules is able to perform memory tasks effectively (Mel 1994).

To provide theoretical justification for such reduced models, we developed an equivalent cable model for active dendrites, comprising Rall's model for passive trees as a special case. Two empirical reduction methods (Clements and Redman 1989; Bush and Sejnowski 1993) were compared with respect to our findings. The reduction process has been demonstrated by simulations of an arbitrarily constructed and a reconstructed, realistic neuronal tree the segments of which were modelled by the FitzHugh-Nagumo system.

In the second part of the paper we compared three morphological tree types of reconstructed neurons. Using the reduction method, different diameter functions of the corresponding equivalent cables were obtained. Depending on the geometric type of the diameter profile the dendritic tree is either able to actively propagate action potentials, or it behaves as in the passive case, in spite of the presence of active channels.

This result is of special interest in the light of recent findings on spike propagation in dendrites. Stuart et al. (1997) observed that dendrites of pyramidal cells are able to boost antidromic spike propagation while failing to support dendritic spike initiation. One explanation has been based on the assumption of an inhomogeneous distribution of active channels (Mainen et al. 1995). Our results show, however, that purely geometric factors might suffice to explain the experimental findings in Stuart et al. (1997).

A functional consequence of the ability for antidromic spike propagation is the way synaptic learning can incorporate the actual activation state of the axon hillock. If the cell is able to perform antidromic excitation spread, then the synapses can incorporate the current 'output' of the cell, whereas otherwise only the local excitation state can influence synaptic plasticity.

Another point worthy of mention here is the ability of a dendritic tree to work as a coincidence detector, instead of simply integrating synaptic input (König et al. 1996). For this, a fine time resolution of the cell is necessary to discriminate the time differences of incoming signals. This could be done in thin distal dendrites, even for the typically high time constants of most neurons (Agmon-Snir and Segev 1993). However, this could only be of functional significance at the soma if dendritic spikes are able to propagate to the soma (Softy 1994). Therefore, the role of a neuron as coincidence detector may depend on the morphological tree type described by the Q-parameter of our model.

With this reduced model the analysis and simulation of voltage spread in rather realistically modelled neurons can be distinctly simplified. It could therefore be helpful in closing the gap between the strongly simplified neuron models without spatial structure, as used in artificial neural networks, and the complex compartment models described by hundreds or thousands of coupled differential equations.

Acknowledgement. This work was supported by the Deutsche Forschungsgemeinschaft, grant no. SCHI 333/4-1.

Appendix A. Nonlinear cable equations

A.1 Hodgkin-Huxley model

The ionic current is determined by three conductances of which two are voltage-dependent (Hodgkin and Huxley 1952).

$$\begin{aligned} j_i &= j_{\mathrm{Na}} + j_{\mathrm{K}} + j_{\mathrm{L}} \\ &= g_{\mathrm{Na}}(V - E_{\mathrm{Na}}) + g_{\mathrm{K}}(V - E_{\mathrm{K}}) + g_{\mathrm{L}}(V - E_{\mathrm{L}}) \\ &= m^3 h \hat{g}_{\mathrm{Na}}(V - E_{\mathrm{Na}}) + n^4 \hat{g}_{\mathrm{K}}(V - E_{\mathrm{K}}) + g_{\mathrm{L}}(V - E_{\mathrm{L}}) \end{aligned} \tag{A.1}$$

Here the constants $\hat{g}_{\mathrm{Na}}$, $\hat{g}_{\mathrm{K}}$ are the maximal conductance values of the sodium and potassium channels and g_{L} is the (constant) value of the passive leak conductance. $u_1 = m$ and $u_2 = h$ are the activation and inactivation variables for sodium, $u_3 = n$ is the activation variable for potassium, which satisfy the condition $0 < m, n, h < 1$ and the following differential equations

$$\begin{aligned} \frac{\partial m}{\partial t} &= f_1 = \alpha_m(1 - m) - \beta_m m \\ \frac{\partial n}{\partial t} &= f_2 = \alpha_n(1 - n) - \beta_n n \\ \frac{\partial h}{\partial t} &= f_3 = \alpha_h(1 - h) - \beta_h h \end{aligned}$$

where α_m, β_m, α_n, β_n, α_h, β_h are empirical functions of the voltage V.

The leak conductance $g_{\mathrm{L}}(x)$ yields, according to (4),

$$g_{\mathrm{L}}(x) = G_{\mathrm{L}} \pi d(x) \sqrt{1 + \frac{1}{4}\left(\frac{\mathrm{d}d}{\mathrm{d}x}\right)^2}$$

Equation (A.1) can be rewritten as

$$\begin{aligned} j_i &= g f_0(V, m, n, h) \\ &= g_{\mathrm{L}}(x)\left(\frac{G_{\mathrm{Na}}}{G_{\mathrm{L}}} m^3 h (V - E_{\mathrm{Na}}) \right. \\ &\quad \left. + \frac{G_{\mathrm{K}}}{G_{\mathrm{L}}} n^4 (V - E_{\mathrm{K}}) + (V - E_{\mathrm{L}})\right) \end{aligned}$$

where G_{Na}, G_{K} and G_{L} are the specific (maximal) membrane conductances of the corresponding ion channels. Then the part of the current dependent on the segment diameter, j_i, is separated from the voltage-dependent part corresponding to the general cable equation (3).

A.2 FitzHugh-Nagumo model

Here the cable equation (3) yields (FitzHugh 1969)

$$\begin{aligned} \frac{\partial}{\partial x}\left(\frac{1}{r_a}\frac{\partial V}{\partial x}\right) - c\frac{\partial V}{\partial t} &= g f_0 = g(h(V) + u) \\ \frac{\partial u}{\partial t} &= \alpha V - \beta u \end{aligned} \tag{A.2}$$

with resting potential equal to zero and cubic $h(V) = V(1 - V/V_1)(1 - V/V_2)$ where $0 < V_1 < V_2$ are the roots of h. The constants α and β are positive so that u acts as a variable, which takes the system from the excited state (near V_2) back to the resting state $u = 0$.

Appendix B. Proof of Theorem 1 (equivalent cable theorem)

We assume that the conditions of Theorem 1 are satisfied for the neuron being considered and an equivalent cable is constructed according to these [see particularly (14) and (15)]. Then we show here the real equivalence of this cable in the sense of Definition 2 using as map T_{eq} the projection map $T_{\text{eq}}(X_\pi) = X$.

Firstly, Condition 2 guarantees that T_{eq} is bijective on any path through the neuron — the first point of Definition 2.

We can further state that any general voltage solution of the equivalent cable yields a general solution for all segments $\pi = (K, L)$ — limited to the corresponding space interval $[X_K, X_L]$. This follows from the assumption that the relevant parameters in the normalized cable equations (7) are equal for all tree segments: (7a) and (7c) are the same for all segments because of Condition 4 of the theorem and analogue (7b) by means of Conditions 1 and 3.

If we therefore define the special voltage solution at any segment π to equal the special solution V of the equivalent cable $(\forall T \geq 0 : V_\pi(X_\pi, T) = V(T_{\text{eq}}(X_\pi), T)$ according to (12), Definition 2, the system of cable equations of the tree is satisfied as well. To verify that this voltage distribution V_π is a correct special solution of the tree we have to prove that the boundary conditions (9) at any node K are satisfied when they are satisfied for the input sites of the equivalent cable at $X = X_K$. For this the axial current in any segment π has to be computed [see (8)]:

$$\begin{aligned} j_{a\pi}(X_\pi, T) &= -\sqrt{\frac{g_\pi(X_\pi)}{r_{a\pi}(X_\pi)}}\frac{\partial V}{\partial X} \overset{(14)}{=} -B_\pi\sqrt{\frac{g_{\text{eq}}(X)}{r_{a\text{eq}}(X)}}\frac{\partial V}{\partial X} \\ &= B_\pi j_{a\text{eq}}(X, T) \end{aligned} \tag{B.1}$$

From the generalized branching rule (14) and (15) it follows that for any electrotonic distance X the sum over all B_π equals 1 by induction over all nodes (Ohme 1996):

$$\sum_{\pi=(K,L)|X\in(X_K,X_L]} B_\pi = 1 \tag{B.2}$$

With this we get for the relation between the input currents in node K (at distance X_K from the tree soma) and into the equivalent cable (at distance $X = X_K$ from the soma of the equivalent cable) with $\pi = \mathscr{PS}(K)$:

$$I_K = B_\pi I_X^{\text{eq}} \tag{B.3}$$

resulting from the definition (17) of I_X^{eq} and equation (16) of Condition 5.

Inserting (B.1) and (B.3), the boundary condition (9) at node K yields (with $\pi = \mathscr{PS}(K)$ and denoting the left and right limit by ± 0 respectively):

$$\begin{aligned} &I_K + \sum_{\pi'\in\mathscr{CS}(K)} j_{a\pi'}(X_K, T) - j_{a\pi}(X_K, T) \\ &= B_\pi I_X^{\text{eq}} + \sum_{\pi'\in\mathscr{CS}(K)} B_{\pi'} j_{a\text{eq}}(X + 0, T) - B_\pi j_{a\text{eq}}(X - 0, T) \\ &\overset{(15)}{=} B_\pi\Big(I_X^{\text{eq}} + j_{a\text{eq}}(X + 0, T) - j_{a\text{eq}}(X - 0, T)\Big) = 0 \end{aligned}$$

which follows according to our premise from Kirchhoff's first law applied to the equivalent cable at input site X. Therefore, the voltage distribution constructed from the voltage solution of the equivalent cable by means of T_{eq} gives a correct solution for the original tree.

To complete the proof it remains for us to show that the sum of axial current flowing through all segments at points X_π with the same image $X = T_{\text{eq}}(X_\pi)$ (i.e. at the same electrotonic distance from soma) is equal to the axial current of the equivalent cable at X [cf. (13)]:

$$\begin{aligned} \sum_{\pi=(K,L)|X\in(X_K,X_L]} j_{a\pi}(X, T) &\overset{(B.1)}{=} \sum_{\pi=(K,L)|X\in(X_K,X_L]} B_\pi j_{a_{\text{eq}}}(X, T) \\ &\overset{(B.2)}{=} j_{a_{\text{eq}}}(X, T) \end{aligned}$$

References

Agmon-Snir H, Segev I (1993) Signal delay and input synchronization in passive dendritic structures. J Neurophysiol 70:2066–2085

Bunow B, Segev I, Fleshman JW (1985) Modeling the electrical behavior of anatomically complex neurons using a network analysis program: excitable membrane. Biol Cybern 53:41–56

Bush PC, Sejnowski TJ (1993) Reduced compartment models of neocortical pyramidal cells. J Neurosci Methods 46:159–166

Clements JD, Redman SJ (1989) Cable properties of cat spinal motoneurones measured by combining voltage clamp, current clamp and intracellular staining. J Physiol (Lond) 409:63–87

FitzHugh R (1969) Mathematical models of excitation and propagation in nerve. In: Schwan HP (ed) Biological Engineering. McGraw-Hill, New York, pp 1–85

Fleshman JW, Segev I, Burke RB (1988) Electrotonic architecture of type-identified alpha-motoneurons in the cat spinal cord. J Neurophysiol 60:60–85

Hodgkin AL, Huxley AF (1952) A quantitative description of membrane current and its application to conduction and excitation in nerve. J Physiol (Lond) 117:500–544

Holmes WR, Rall W 1992) Estimating the electrotonic structure of neurons with compartmental models. J Neurophysiol 68:1438–1452

Jack JJB, Noble D, Tsien RW (1983) Electric current flow in excitable cells. Oxford University Press, Oxford

König P, Engel AK, Singer W (1996) Integrator or coincidence detector? The role of the cortical neuron revisited. Trends Neurosci 19:130–137

Mainen ZF, Sejnowski TJ (1996) Influence of dendritic structure on firing pattern in model neocortical neurons. Nature 382:363–366

Mainen ZF, Joerges J, Huguenard JR, Sejnowski TJ (1995) A model of spike initiation in neocortical pyramidal neurons. Neuron 15:1427–1439

Mainen ZF, Carnevale NT, Zador AM, Claiborne BJ, Brown TH (1996) Electrotonic architecture of hippocampal ca1 pyramidal neurons based on three-dimensional reconstructions. J Neurophysiol, 76:1904–1923

Mel BW (1994) Information processing in dendritic trees. Neural Comput 6:1031–1085

Ohme M (1996) Modellierung der neuronalen Signalverarbeitung mittels kontinuierlicher Kabelmodelle. Dissertation, University of Leipzig, Department of Computer Science

Ohme M, Schierwagen AK (1993) Influence of geometry on velocity and frequency of action potential propagation in excitable neural fibres. In: Elsner N, Heisenberg M (eds) Gen — Gehirn — Verhalten: Proceedings of the 21th Göttingen neurobiology conference, Thieme, Stuttgart

Ohme M, Schierwagen AK (1994) Heterosynaptic inputs in dendritic trees. In: Elsner N, Heisenberg M (eds) Sensorische Transduktion: Proceedings of the 22th Göttingen neurobiology conference, Thieme, Stuttgart

Ohme M, Schierwagen AK (1996a) A method for analysing transients in dendritic trees with nonuniform segments. In: Trappl R (ed) Cybernetics and systems '96. Austrian Society for Cybernetic Studies, Vienna pp 542–547

Ohme M, Schierwagen AK (1996b) A reduced model for dendritic trees with active membrane. In: von der Malsburg C, von Seelen W, Vorbrüggen JC, Sendhoff B (eds) Artificial neural networks — ICANN 96. Springer, Berlin Heidelberg New York pp 691–696

Ohme M, Schierwagen AK (1997) Modelling dendritic trees with active membrane. In: Elsner N, Wässle H (eds) From membrane to mind: Proceedings of the 25th Göttingen neurobiology conference. Thieme, Stuttgart

Rall W (1962) Theory of physiological properties of dendrites. Ann N Y Acad Sci 96:1071–1092

Rapp M, Segev I, Yarom Y (1994) Physiology, morphology and detailed passive models of guinea-pig cerebellar Purkinje cells. J Physiol (Lond) 474:101–118

Rinzel J, Terman D (1982) Propagation phenomena in a bistable reaction-diffusion system. SIAM J Appl Math, 42:1111–1136

Schierwagen AK (1989) A non-uniform equivalent cable model of membrane voltage changes in a passive dendritic tree. J Theor Biol 141:159–179

Schierwagen AK (1991) Travelling wave solutions of a simple nerve conduction equation for inhomogeneous axons. In: Holden AV, Markus M, Othmer H (eds) Nonlinear wave processes in excitable media, Manchester University Press, Manchester, pp 107–114

Schierwagen AK (1994) Exploring the computational capabilities of single neurons by continuous cable modelling. In: van Pelt J, Corner MA, Uylings HBM, Lopes da Silva FH (eds) The selforganizing brain — from growth cones to functional networks. (Progress in brain research, vol 102) Elsevier, Amsterdam, pp 151–167

Schierwagen AK, Grantyn R (1986) Quantitative morphological analysis of deep superior colliculus neurons stained intracellularly with HRP in the cat. J Hirnforsch 27:611–623

Segev I, Fleshman JW, Miller JP, Bunow B (1995) Modeling the electrical behavior of anatomically complex neurons using a network analysis program: passive membrane. Biol Cybern 53:27–40

Segev I (1995) Dendritic processing. In: Arbib MA (ed) The handbook of brain theory and neural networks, MIT Press, Cambridge, Mass, pp 282–289

Softky W (1994) Sub-millisecond coincidence detection in active dendritic trees. Neuroscience, 58:13–41

Stratford K, Mason A, Larkman A, Major G, Jack JJB (1989) The modelling of pyramidal neurons in the visual cortex. In: Durbin R, Miall C, Mitchison G (eds) The computing neuron, Addison-Wesley, London, pp 296–321

Stuart G, Spruston N, Sakmann B, Hausser M (1997) Action potential initiation and backpropagation in neurons of the mammalian CNS. Trends Neurosci 3:125–131

van Pelt J (1992) A simple vector implementation of the Laplace-transformed cable equations in passive dendritic trees. Biol Cybern 68:15–21